Zircon U-Pb Age, Sr-Nd-Hf Isotopic Characteristics of Baiyinhushuo Adakite in Inner Mongolia:Implications for Tectonic Evolution

Yuxu Fan *, Qinghui Xiao , Yang Cheng , Yan Li

Posted Date: 11 June 2024

doi: 10.20944/preprints202406.0702.v1

Keywords: Paleo-Asian Ocean; Adakite; Zircon chronology; Sr-Nd isotope; Subducted slab

Article

Zircon U-Pb Age, Sr-Nd-Hf Isotopic Characteristics of Baiyinhushuo Adakite in Inner Mongolia:Implications for Tectonic Evolution

Yuxu Fan [1,2,*], Qinghui Xiao [2] and Yang Cheng [3] and Yan Li [3]

[1] General Prospecting Institute of China National Administration of Coal Geology, Beijing 100039
[2] Institute of Geology, Chinese academy of Geological Sciences, Beijing 100037
[3] Institute of Mineral Resources, China Metallurgical Geology Bureau, Beijing 101300
* Correspondence: Correspondence: fanyuxu.123@163.com

Abstract: The petrogenesis and geodynamic implications of the early Paleozoic adakitic rocks in the east of Inner Mongolia remain topics of debate. In this study, petrology, zircon U–Pb age and Lu–Hf isotopic composition, whole-rock geochemistry and Sr–Nd isotopes from adakitic rocks. Zircon U–Pb dating results demonstrate that the formation age is 242.8±1.0Ma, 247Ma, which is the product of Early Triassic magmatism. Petrology and geochemical study have shown that the granodiorite have high SiO_2 (66.93% ~69.40%), Al_2O_3(15.37% ~ 15.43%), MgO (1.35% ~1.55%), with LREE enrichment and HREE deficit, and they have high Sr, low Y. and high Sr/Y ratios, showing typical signatures of adakitic rocks. The $\varepsilon_{Hf}(t)$ values of zircon vary between +11.3 and +13.8, with a low whole-rock ($^{87}Sr/^{86}Sr$)i (0.703382)and positive $\varepsilon_{Nd}(t)$ values, the average $Mg^{\#}$ of the rock is 56.14, suggesting that adakite derived from partial melting of MORB, and magma interaction with the mantle. Comprehensive analysis suggests that during the Late Permian to Early Triassic, the subducted slab of the Paleo-Asian Ocean broke off, and the residual oceanic slab preserved in the mantle beneath the subduction zone underwent partial melting, generating adakitic magma.

Keywords: Paleo-Asian Ocean; Adakite; zircon chronology; Sr-Nd isotope; subducted slab

1. Introduction

The southeastern segment of the Central Asian Orogenic Belt（CAOB）is sandwiched between the Siberian, North China, and Pacific plates. It is the longest-known Phanerozoic accretion orogenic belt, with the complex tectonic-magmatic processes. The widespread occurrence of Paleozoic ophiolite, subduction-accretion mélanges, island arcs, micro-continental blocks, and complex magmatic rocks within the belt is closely related to the evolution of the Paleo-Asian Ocean. This region has long been the focus of attention from the domestic and international geological community, and has achieved a series of important results [1–10]. The Baiyinhushuo area in Inner Mongolia, located in the southeastern part of the CAOB, is characterized by the development of multiple ophiolites and abundant magmatic rocks. It is considered the place where the Paleo-Asian Ocean trench-arc-basin system developed and where the final closure of the CAOB [11–13]. The region has undergone a complex tectonic evolution and serves as a natural laboratory for reaching the accretionary orogenesis of the CAOB.

At present, a large number of late Permian to early Triassic adakites have been found on both sides of the Xar-Moron River suture zone, which are considered to be magmatism of crustal thickening and melting during the evolution of the accretionary orogeny to the final collision [7–10,14,15], and some experts believe that it was formed by the melting of residual Paleo-Asian Ocean subducted slabs [16,17]. Previous studies have shown that the Central Asian orogenic belt have experienced the evolutionary stages from subduction to collision during the late Permian to the early Triassic [14,18,19], is a transitional period in tectonic evolution of the eastern part of the CAOB. In this paper, detailed zircon U-Pb dating, zircon in-situ Lu-Hf isotope and whole rock Sr-Nd isotope

Preprints.org (www.preprints.org) | NOT PEER-REVIEWED | Posted: 11 June 2024 doi:10.20944/preprints202406.0702.v1

analysis were carried out on the granodiorite intrusion in Baiyinhushuo. The genetic types and tectonic environment of the rocks were discussed, which provided constraints for the late Paleozoic tectonic evolution, and provided important information for the study of the tectonic-magmatic evolution process from subduction to collision.

2. Geological Setting and Samples

Baiyinhushuo is located in the northern part of Xi Ujimqin, which is located on the southeastern margin of the CAOB (Figure 1a), north of the Solonker-Xar Moron River ophiolite belt and south of the Erenhot-Hegenshan ophiolite belt (Figure 1b). In the Paleozoic period, it experienced multi-stage subduction and accretion of the Paleo-Asian Ocean, which is a typical accretionary orogenic belt [2,3]. The exposed strata are mainly the Late Paleozoic Amushan Formation and Gegenaobao Formation, as well as the Early Cretaceous Baiyingaolao Formation and the Quaternary sediments. The main lithology of Gegenaobao Formation is siltstone and fine siltstone, which experienced strong metamorphism. The metamorphism of the clastic rocks is mainly carbonatization, silicification and hornblende.

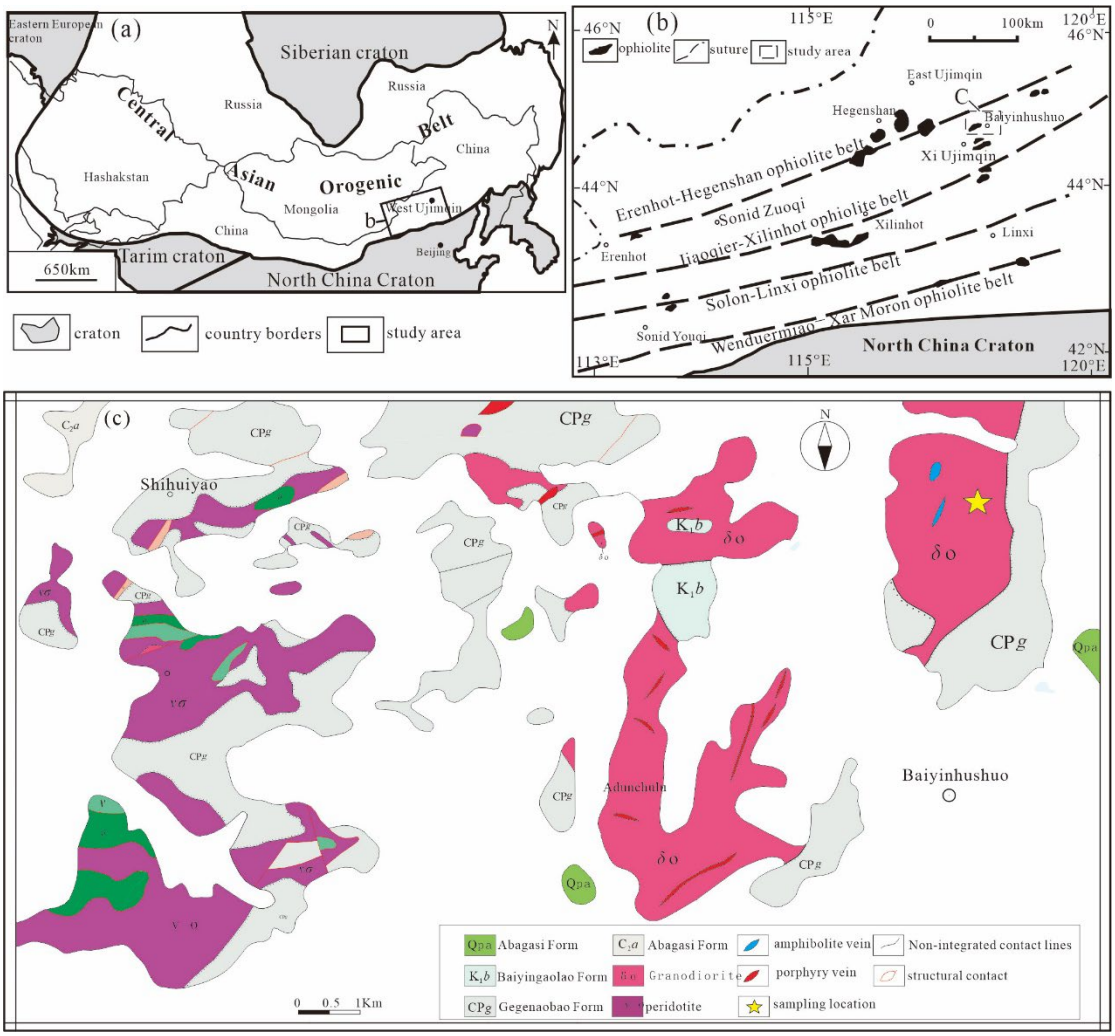

Figure 1. (**a**) Distribution range of the Central Asian Orogenic Belt (CAOB; modified from [9]). (**b**) Sketched tectonic map of the adakite in Baiyinhushuo, Inner Mongolia (modified from [20,21]). (**c**) simplified geologic map of the study area.

The magmatic rocks in the study area are relatively developed and have a large outcropping area., the ophiolite of Wusinihei is located in the western part of the study area. Baiyinhushuo granodiorite intrude into Gegenaobao Formation. The intermediate-acidic dikes are widely

 doi:10.20944/preprints202406.0702.v1

distributed in the Baiyinhushuo granodiorite, Which the main lithologies are quartz-diorite porphyrite, granite porphyry and quartz porphyry, and early Cretaceous andesite, rhyolite and other volcanic rocks can be found in some places.

The granodiorite is overall grayish-white, massive, medium-coarse-grained structure, and the rock can be seen slight fractured (Figure 2). It is mainly composed of plagioclase (75-80%), quartz (15%±), K-feldspar (5-10%), smectite (2-3%), hornblende (2-3%). Observed under the microscope, plagioclase is subhedral and haphazardly distributed,, which the size is generally 1-2mm, part of the 2-4mm, with the development of lamellar double crystals, and some particles showed an obvious ring structure. Quartz for it shape granular structure, the size of the general 0.5-1mm, part of 0.2-0.5mm, a small portion of 0.1-0.2mm, gap-filling distribution, the surface is fresh and clean, wave-like extinction is common, can be seen band extinction. Potassium feldspar semiautomorphic plate-like, size of about 0.5-1mm, part 1-1.5mm, haphazard distribution, light earthy, dirty surface. Hornblende semi-autonomous columnar, size generally 0.5-1mm, a few 1-1.5mm, haphazardly distributed. Black mica is flaky, flake diameter 0.5-1mm, part 1-1.5mm, haphazard distribution, local account of alteration, visible green cordite, chlorite.

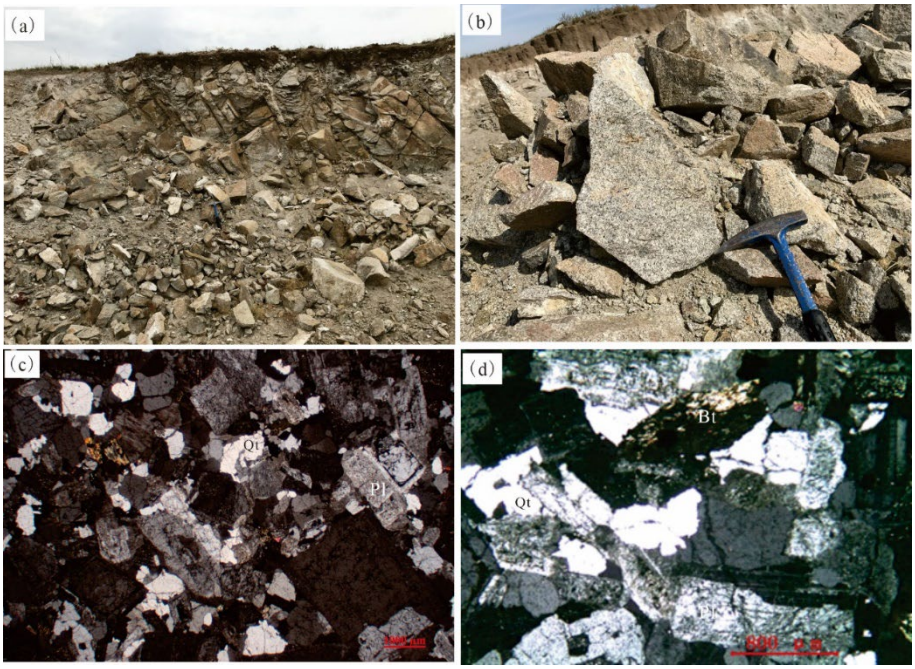

Figure 2. Field outcrop (**a**,**b**) and photomicrograph (**c**,**d**) of granodiorite.

3. Analytical Methods

3.1. Whole-Rock Major and Trace Element

The fresh rock samples were crushed into 200 mesh without pollution and the powder samples were sent to the State Key Laboratory of Mineral Deposits Research, Nanjing University(NJU) for major and trace element analysis. The major elements were tested by XRF method using ARL 9900 X-ray fluorescence spectrometer (XRF). The working voltage of the X-ray was 40 kV and the current was 75mA. When the sample concentration was >1.0%, the relative error of analysis was +1%. When the sample concentration was <1.0%, the relative error was +10%. Trace elements and rare earth elements were determined by high-resolution inductively coupled plasma mass spectr ometry. The samples were first chemically dissolved in a high-pressure reactor and then analyzed by plasma mass spectrometer (Instrument Model: ELEMENT-2) with a relative error of approximately 2%.

 doi:10.20944/preprints202406.0702.v1

3.2. Zircon LA-ICP-MS U-Pb Dating

Strictly avoiding pollution, zircon single minerals were selected through crushing, sorting, and picking out under a binocular microscope with no cracks on the surface, smooth and intact. Then the samples were made into targets with Canadian resin and photographed with cathodoluminescence by a scanning electron microscope. Zircon U-Pb isotopic dating was completed at the China University of Geosciences (Beijing), using the experimental method of LA-ICP-MS in-situ dating and the experimental instruments of 193nm excimer laser and inductively coupled plasma mass spectrometer (Instrument Model: Thermo Xseries2). The mass spectrometer used He gas as the carrier gas, and the laser spot diameter used in the analysis was 32μm with a frequency of 6Hz. The data processing and concordia plot drawing of zircon U-Pb dating were obtained by ICPMSDataCal program [22] and Isoplot 3.0 program [23].

3.3. Whole-Rock Sr-Nd Isotopes and Zircon Lu-Hf Isotopes

Whole-rock Sr-Nd isotope analyses were determined by Triton TI surface thermal ionization mass spectrometry (TIMS) at the State Key Laboratory of Mineral Deposits Research, Nanjing University. A 200-mesh rock powder sample was taken, dried and completely dissolved in a mixed acid of HF+HNO3, and Sr and Nd were separated and purified using a cation exchange resin. The Sr and Nd isotope ratios were corrected by mass fractionation using $^{86}Sr/^{88}Sr=0.1194$ and $^{146}Nd/^{144}Nd=0.7219$.

The analysis of zircon Lu-Hf isotopes was completed in the Key Laboratory of Continental Dynamics of Ministry of Natural Resources, using Neptune Plus multi-reception plasma mass spectrometer and Geo Las Pro193nm laser ablation system (LA-MC-ICP-MS). Depending on the size of the zircon, the diameter of the laser ablation system was 44 μm, and the international standard for zircon, GJ-1, was used as the reference material. Detailed operation conditions and analysis procedures of relevant instruments can be found in Hou et al. [24]. The weighted average values of $n(^{176}Hf)/n(^{177}Hf)$ tests for zircon standard GJ-1 during the analysis were 0.282008 ± 0.000050 (2σ), respectively. For the calculation of the initial $^{176}Hf/^{177}Hf$, a decay constant of $1.865 \times 10^{-11}a^{-1}$ [25] was used for Lu, and $\varepsilon_{Hf}(t)$ values were calculated using the spherical meteorite Hf isotope values of $n(^{176}Lu)/n(^{177}Hf) = 0.0332$, $n(^{176}Hf)/n(^{177}Hf) = 0.282772$ [26].

4. Analytical Results

4.1. Chronological Characteristics

The zircons of the Baiyinhushuo granodiorite are well crystalline, with zircon grain sizes ranging from 0.08 to 0.25 mm, generally authomorphic-semi-authomorphic, and colorless-light yellow. The Th/U ratios of the zircons range from 0.40 to 1.08, with an average of 0.55 (Table 1), and the cathodoluminescence photographs show the obvious oscillation zones and fan-shaped ring zones (Fig. 3), indicating that they were all magmatic crystallization zircons. [27,28]. Among the 25 zircons points, 19 zircons exhibit relatively concentrated ages and are located near the concordance line, while a few samples show poor concordance in their age data. The individual zircon $^{206}Pb/^{238}U$ ages are listed in Table 1, and the zircon concordant age is 242.8 ± 1.0 Ma (MSWD=2.0), indicating they are products of Early Triassic magmatic activity (Figure 4).

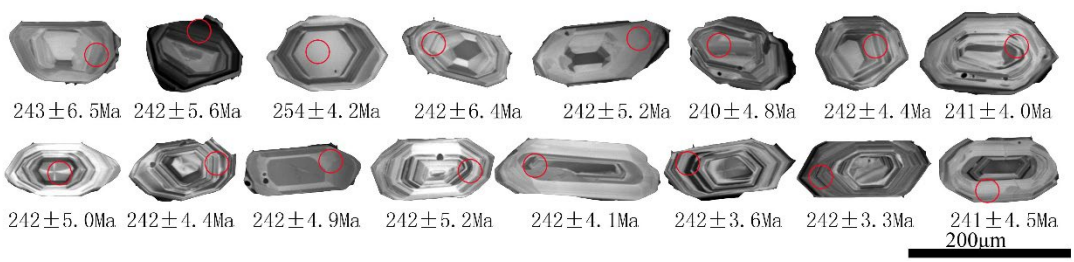

 doi:10.20944/preprints202406.0702.v1

Figure 3. Representative CL images of analyzed zircons. Ages (Ma) and analysis spots (cycle) are marked on the zircons.

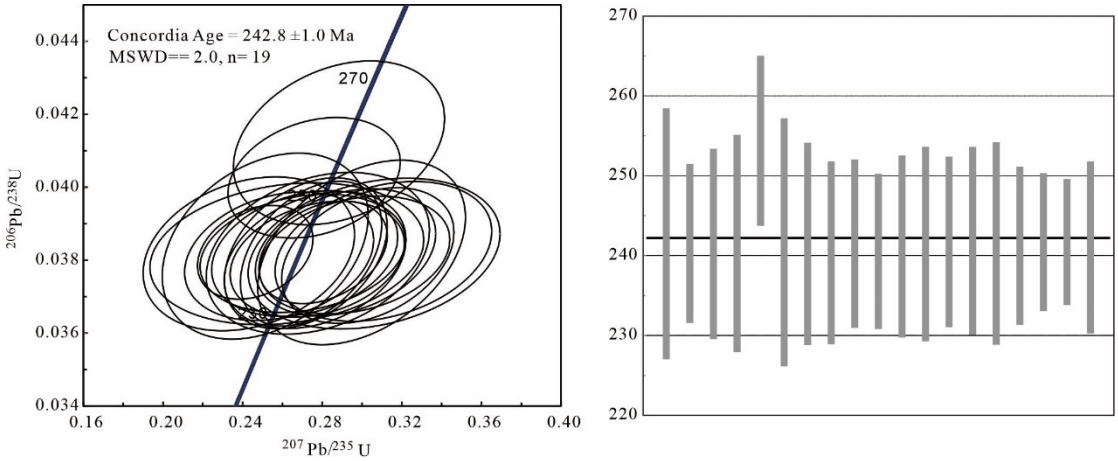

Figure 4. Concordia and weight diagrams of U-Pb ages of zircons for the Granodiorite.

Table 1. LA-ICP-MS zircon U-Pb dating results of the Baiyinhushuo.

spot	Pb	Th	U	isotope ratio						age					
				$^{207}Pb/^{206}Pb$		$^{207}Pb/^{235}U$		$^{206}Pb/^{238}U$		$^{207}Pb/^{206}Pb$		$^{207}Pb/^{235}U$		$^{206}Pb/^{238}U$	
HS17-05-1	9.20	81.59	196.24	0.0549	0.0065	0.2612	0.0243	0.0371	0.0009	409.3	265.6	235.6	19.5	234.7	5.8
HS17-05-2	10.81	96.49	215.68	0.0516	0.0057	0.2746	0.0281	0.0390	0.0009	264.9	237.0	246.3	22.4	246.6	5.6
HS17-05-3	11.54	105.51	266.05	0.0514	0.0056	0.2749	0.0320	0.0390	0.0009	257.5	242.6	246.6	25.5	246.5	5.8
HS17-05-7	17.52	210.71	323.19	0.0523	0.0048	0.2818	0.0251	0.0397	0.0010	298.2	211.1	252.1	19.9	250.9	6.2
HS17-05-9	12.65	117.88	238.69	0.0500	0.0050	0.2885	0.0265	0.0410	0.0010	194.5	218.5	257.4	20.9	259.0	6.1
HS17-05-10	9.89	104.35	215.33	0.0542	0.0049	0.2753	0.0232	0.0374	0.0012	388.9	203.7	246.9	18.5	236.5	7.3
HS17-05-11	8.67	65.99	168.49	0.0558	0.0061	0.3106	0.0286	0.0428	0.0012	442.6	272.2	274.7	22.1	270.5	7.5
HS17-05-12	25.16	298.49	488.14	0.0505	0.0033	0.2698	0.0175	0.0386	0.0008	220.4	153.7	242.6	14.0	244.1	4.7
HS17-05-13	17.12	185.40	334.21	0.0505	0.0038	0.2696	0.0203	0.0384	0.0008	220.4	177.8	242.4	16.2	243.2	5.1
HS17-05-14	12.17	111.35	258.52	0.0510	0.0048	0.2702	0.0230	0.0386	0.0008	242.7	216.6	242.9	18.4	244.5	4.9
HS17-05-15	12.50	103.26	267.82	0.0523	0.0045	0.3101	0.0255	0.0431	0.0011	301.9	191.6	274.3	19.8	272.0	6.5
HS17-05-17	33.82	553.50	483.04	0.0523	0.0034	0.2844	0.0168	0.0402	0.0008	298.2	150.0	254.1	13.3	254.1	5.0
HS17-05-18	22.37	227.49	442.93	0.0526	0.0034	0.2846	0.0181	0.0388	0.0008	309.3	148.1	254.3	14.3	245.5	4.7
HS17-05-20	10.94	104.53	223.74	0.0547	0.0054	0.2843	0.0259	0.0389	0.0010	466.7	222.2	254.1	20.5	245.9	6.0
HS17-05-21	24.59	317.06	463.84	0.0511	0.0034	0.2593	0.0167	0.0371	0.0008	242.7	153.7	234.1	13.5	234.8	5.0
HS17-05-22	16.22	186.03	314.59	0.0507	0.0045	0.2674	0.0226	0.0382	0.0008	227.8	207.4	240.6	18.1	241.6	4.8
HS17-05-23	36.25	408.73	719.38	0.0521	0.0030	0.2739	0.0163	0.0381	0.0007	287.1	133.3	245.8	13.0	241.2	4.6

 doi:10.20944/preprints202406.0702.v1

HS17-05-24	26.68	234.30	617.82	0.0497	0.0035	0.2586	0.0176	0.0377	0.0007	189.0	167.6	233.5	14.2	238.6	4.6
HS17-05-25	22.14	269.19	451.68	0.0507	0.0038	0.2629	0.0198	0.0375	0.0008	227.8	175.9	237.0	15.9	237.1	4.8

4.2. Major and Trace Elements

The petrochemical data of Baiyinhushuo granodiorite are shown in Table 2. The SiO_2 content of the granodiorite is 66.93%-69.40%, with an average of 67.75%. The Na_2O content is 4.35%-5.45%, with an average of 4.63%. The K_2O content is 2.48%-2.95%, with an average of 2.60%, and the Na_2O/K_2O ranges from 1.56 to 2.05. Al_2O_3 content was 15.13%-15.53% with an average of 15.39%. In the TAS diagram, the samples fall in the granodiorite fields, subalkaline magmatic series (Figure 5a,d). The total alkali (Na_2O+K_2O) were 6.82-8.12%, showed calc–alkaline to high-K calc–alkaline series (Figure 5b). The Al_2O_3 content of 11.45-14.11% were low, which the A/CNK value were 0.94-1.01, and the A/NK value ranges from 1.30-1.54, in the A/NK–A/CNK diagram (Figure 5c), the samples fall in the quasialuminum field (Figure 5c).

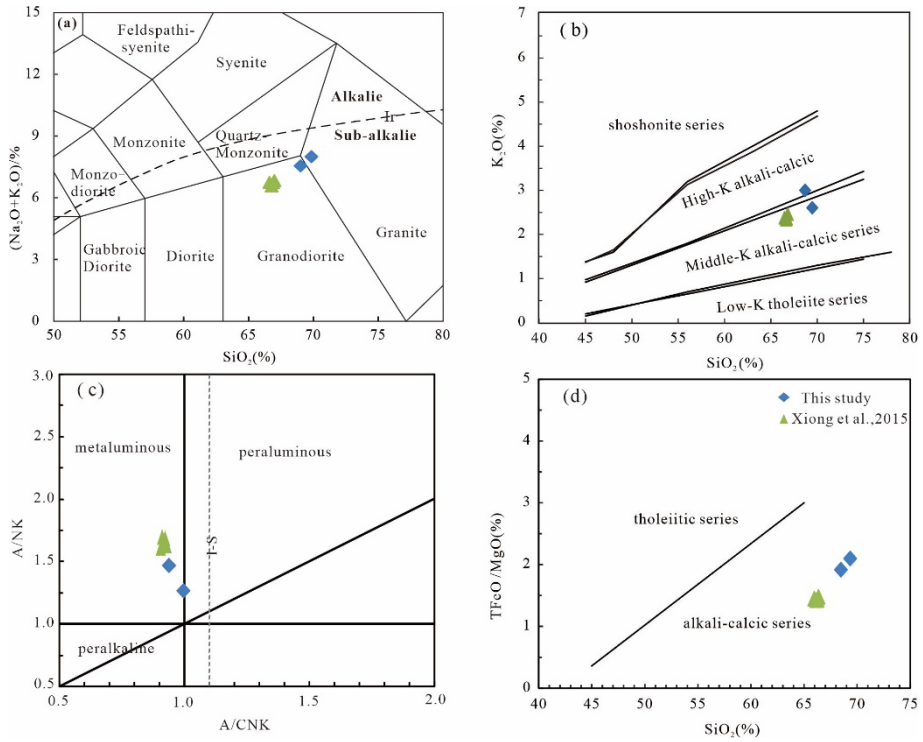

Figure 5. (**a**). Total alkalis- SiO_2 (TAS) [29], (**b**). ANK-ACNK plot [30], (**c**). K_2O-SiO_2[31], (**d**). TFeO/MgO-SiO_2 diagram [32].

The ΣREE of the granodiorite are low, with ΣREE contents ranging from 54.39×10^{-6} to 76.84×10^{-6}, they showed a right-leaning chondrite distribution curve with a strong differentiation of light and heavy rare earth elements. The LREE/HREE value was 7.38-10.68, with an average of 8.53; the $(La/Yb)_N$ value was 8.14-13.93, with an average of 10.10; the δEu value was 0.79-1.02, with an overall weak negative Eu anomaly. The trace element primitive mantle spidergram is enriched in large ionic lithophilic elements (LILEs), such as Rb, Ba, Th, U., and depleted in high-field-strength elements (HFSEs), such as Nb, P, Ti. The trace elements have high Sr (424.00×10^{-6}~570.14×10^{-6}), and high Sr/Y (42.79~62.91) (Table 2).

 doi:10.20944/preprints202406.0702.v1

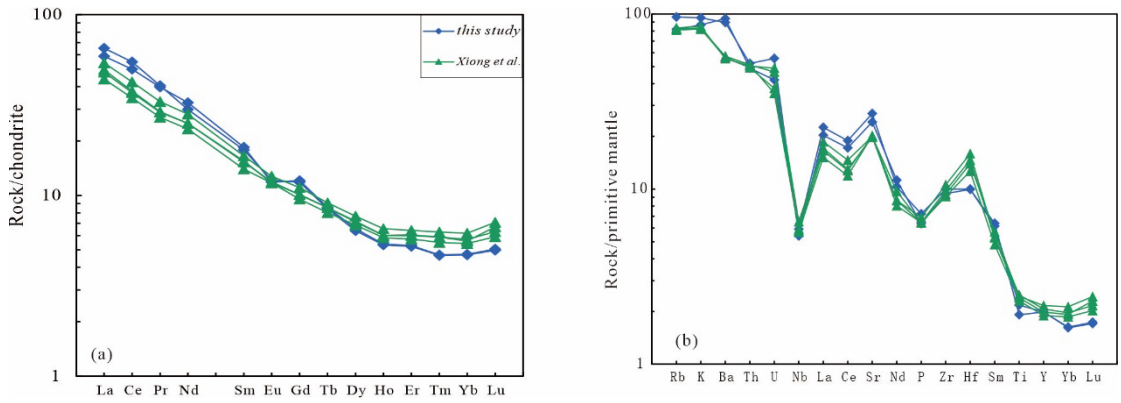

Figure 6. Chondrite-normalized REE pattern and Primitive mantle-normalized trace elements spider diagram [33].

The geochemical composition of the granodiorite sampled in this study is consistent with Xiong et al. [15]. The SiO_2 varies from 66.93% to 69.40%, MgO ranges from 1.35% to 1.55%, and Al_2O_3 is between 15.37% to 15.43%, and the rock is characterized by high Sr, low Y and high Sr/Y, which is consistent with the geochemical characteristics of typical adakites.

4.3. Isotope Geochemical Characterization

The Lu-Hf isotope analysis of zircon shows (Table 3) that the $^{176}Lu/^{177}Hf$ ratio is less than 0.002, indicating that the zircons had extremely low amounts of radiotracer Hf, and that the measured $^{176}Hf/^{177}Hf$ ratios basically represent the Hf isotopic Hf isotopic composition system during crystallization [34]. The variation of $^{176}Hf/^{177}Hf$ of the samples ranges from 0.282943 -0.283014, with an average of 0.282985. The corresponding $\varepsilon_{Hf}(t)$ values range from +11.3 to +13.8, all of which are positive. The depleted mantle model age (T_{DM}) is 334-436 Ma, and the two-stage model age (T_{2DM}) is 389-553 Ma. The $^{87}Rb/^{86}Sr$ and $(^{87}Sr/^{86}Sr)_i$ of the Baiyinhushuo granodiorite sample is low, which the $^{87}Rb/^{86}Sr$ is 0.346558, and the $(^{87}Sr/^{86}Sr)_i$ is 0.703882. $^{147}Sm/^{144}Nd$ is 0.112238, $\varepsilon_{Nd(t)}$ is +7.72, which is a positive value. The two-stage mode age of T_{2DM} is 387 Ma (Table 4).

Table 2. Composition of major elements (%), trace elements ($\times10^{-6}$) and REE ($\times10^{-6}$) of samples from the Granodiorite.

Sample	SiO_2	TiO_2	Al_2O_3	Fe_2O_3	FeO	MnO	MgO	CaO	Na_2O	K_2O	P_2O_5	LOI	TATOL	$Mg^{\#}$	A/CNK
HS17-05	69.40	0.48	15.43	3.07	/	0.05	1.35	1.92	5.45	2.67	0.16	1.39	99.29	46.73	1.01
HS17-09	68.76	0.43	15.37	3.24	/	0.06	1.55	2.90	4.60	2.95	0.14	2.2	99.06	48.87	0.96
DW11-b1*	67.06	0.54	15.13	1.84	1.58	0.04	2.27	3.4	4.35	2.47	0.15	0.82	98.83	61.78	0.95
DW11-43*	66.93	0.53	15.48	1.76	1.49	0.03	2.12	3.52	4.45	2.5	0.14	0.95	98.95	61.55	0.94
DW11-4*	67.22	0.5	15.53	1.38	1.71	0.03	2	3.45	4.46	2.56	0.14	0.98	98.98	56.82	0.95
DW11-6*	67.15	0.52	15.4	1.68	1.51	0.03	2.11	3.47	4.46	2.48	0.14	0.92	98.95	61.12	0.94
Sample	Rb	Ba	Th	U	Nb	Sr	Nd	Zr	Hf	Yb	La	Ce	Pr	Nd	Sm
HS17-05	52	657.55	4.17	0.88	4.21	570.14	13.96	112	3.09	0.80	15.47	33.55	3.85	13.96	2.73
HS17-09	61	625.28	4.44	1.17	3.86	509.54	15.23	105	3.08	0.80	13.96	30.53	3.77	15.23	2.83
DW11-b1	52.5	401.4	4.35	0.98	4.65	416.6	11.67	118.5	4.92	0.97	11.75	23.1	2.76	11.67	2.37
DW11-43	51.9	399.7	4.36	0.74	4.22	421.1	13.15	104.6	4.31	1.05	12.83	25.99	3.14	13.15	2.53
DW11-4	52.9	388.5	4.28	1.03	4.05	425.7	10.89	101.5	3.91	0.92	10.44	21.18	2.57	10.89	2.14
DW11-6	51.3	393.3	4.2	0.79	4.15	424	11.69	109.7	4.53	0.95	11.39	22.67	2.74	11.69	2.34

 doi:10.20944/preprints202406.0702.v1

Sample	Eu	Gd	Tb	Dy	Ho	Er	Tm	Yb	Lu	Y	ΣREE	LREE/HREE	La_N/Yb_N	δEu
HS17-05	0.70	2.43	0.32	1.62	0.30	0.86	0.12	0.80	0.13	9.06	76.84	10.68	13.93	0.83
HS17-09	0.69	2.48	0.32	1.66	0.30	0.87	0.12	0.80	0.13	9.04	73.71	10.00	12.47	0.79
DW11-b1	0.68	2.08	0.32	1.83	0.34	0.99	0.15	0.97	0.16	9.42	59.17	7.65	8.69	0.94
DW11-43	0.74	2.27	0.34	1.95	0.37	1.06	0.16	1.05	0.18	9.84	65.76	7.91	8.76	0.94
DW11-4	0.68	1.96	0.3	1.74	0.33	0.95	0.14	0.92	0.15	8.64	54.39	7.38	8.14	1.02
DW11-6	0.69	2.07	0.32	1.81	0.34	1	0.15	0.95	0.17	9.03	58.33	7.57	8.60	0.96

* data from Xiong et al., 2015;.

Table 3. Zircon Lu-Hf isotopic compositions of the granodiorite.

Spot	t(Ma)	$^{176}Yb/^{177}Hf$	2σ	$^{176}Lu/^{177}Hf$	2σ	$^{176}Hf/^{177}Hf$	2σ	$\varepsilon_{Hf}(0)$	$\varepsilon_{Hf}(t)$	T_{DM}(Ma)	T_{2DM}(Ma)	f(Lu/Hf)s
HS17-05-10	242.8	0.012445	0.000207	0.000465	0.000006	0.283006	0.000017	8.28	13.5	343	405	-0.99
HS17-05-10 (2)	242.8	0.020651	0.000135	0.000779	0.000007	0.282970	0.000020	7.00	12.2	397	491	-0.98
HS17-05-11	242.8	0.022239	0.000562	0.000871	0.000018	0.282982	0.000015	7.44	12.6	381	464	-0.97
HS17-05-13	242.8	0.022755	0.000505	0.000914	0.000021	0.283014	0.000016	8.57	13.8	336	391	-0.97
HS17-05-14	242.8	0.011469	0.000265	0.000470	0.000012	0.282996	0.000016	7.93	13.2	357	428	-0.99
HS17-05-15	242.8	0.019129	0.000328	0.000722	0.000008	0.282951	0.000016	6.34	11.6	423	533	-0.98
HS17-05-3	242.8	0.028464	0.000230	0.001110	0.000007	0.282954	0.000016	6.42	11.6	424	532	-0.97
HS17-05-4	242.8	0.016900	0.000988	0.000670	0.000038	0.283014	0.000018	8.57	13.8	334	389	-0.98
HS17-05-5	242.8	0.017065	0.000089	0.000703	0.000004	0.282999	0.000017	8.02	13.2	356	425	-0.98
HS17-05-6	242.8	0.010922	0.000090	0.000425	0.000003	0.282999	0.000015	8.03	13.3	353	421	-0.99
HS17-05-7	242.8	0.019116	0.000357	0.000741	0.000010	0.282943	0.000015	6.03	11.3	436	553	-0.98
HS17-05-8	242.8	0.021709	0.000173	0.000873	0.000008	0.282972	0.000016	7.09	12.3	395	487	-0.97
HS17-05-9	242.8	0.016488	0.000241	0.000661	0.000008	0.283001	0.000016	8.11	13.3	352	419	-0.98

Table 4. Sr-Nd isotopic compositions of the representative samples for the Baiyinhushuo pluton.

Scheme 87.	Rb (μg/g)	Sr (μg/g)	$^{87}Rb/^{86}Sr$	$^{87}Sr/^{86}Sr(2\sigma)$	$(^{87}Sr/^{86}Sr)_i$	Sm (μg/g)	Nd (μg/g)	$^{147}Sm/^{144}Nd_s$	$^{143}Nd/^{144}Nd_s$	$^{143}Nd/^{144}Nd(t)$	$\varepsilon_{Nd}(0)$	$\varepsilon_{Nd}(t)$	T_{DM2}
HS17-09	60.98	509.54	0.34606	0.705058	0.703882	2.83	15.23	0.1122	0.512900	0.512721	5.10	7.72	387

 doi:10.20944/preprints202406.0702.v1

5. Discussion

5.1. Chronology

The emplacement age of the granodiorite has been controversial. In the 1:250,000 area survey report, the Baiyinhushuo granite was classified as Early Permian. Bao et al. (2007) [35] measured the age from 246 to 216Ma by the method of SHRIMP, and Xiong et al. (2015) [15] reported the zircon U-Pb age of 236.1±3.4 Ma. The present age obtained by zircon LA-ICP-MS in the Baiyinhushuo granodiorite is 242.8±1.0 Ma (MSDW = 2.0), which is Early Triassic.

In the adjacent area, the magma activity was more frequent during the Late Permian Early Triassic. Late Late Permian granodiorites have been found in Seerbeng and Nuhetingshala in the southwest of Xi Ujimqin [16], the Longtoushan pluton and the Zhuanshanzi pluton in the Linxi area (245.6 ± 0.9 Ma, [7]), the Baiyinnuoer Triassic granodiorite as (245.4 ± 1.8 Ma, [36]), and the andesites of Xingfuzhilu Formation in the Linxi area (247 Ma,[17]), and all of them are characterized by typical adakite, suggesting that there was a period of adakic magma eruption during the Late Late-Permian-Early Triassic.

5.2. Petrogenesis of Adakite

The Baiyinhushuo granodiorite, with high Sr content and Sr /Y and La /Yb ratios, is a typical adakite (Figure 7), which has special continental dynamics significance [37]. In recent years, a large number of adakites Late Permian-Early Triassic have been discovered in the southeastern section of the Central Asian orogenic belt, which are distributed along the Xar Moron River suture zone [7,14,19]. Currently, there are three views on the geological background of adakite both sides of the Xar Moron suture zone: one suggests that they drived from the remelting of the Juvenile lower crust [7,8,14,15]; one suggests that subducted slabs broke off, and remained slabs in the mantle were melted and interacted with the mantle [16]; and another viewpoint suggests that the Triassic adakites were caused by plate subduction of the oceanic crust [17].

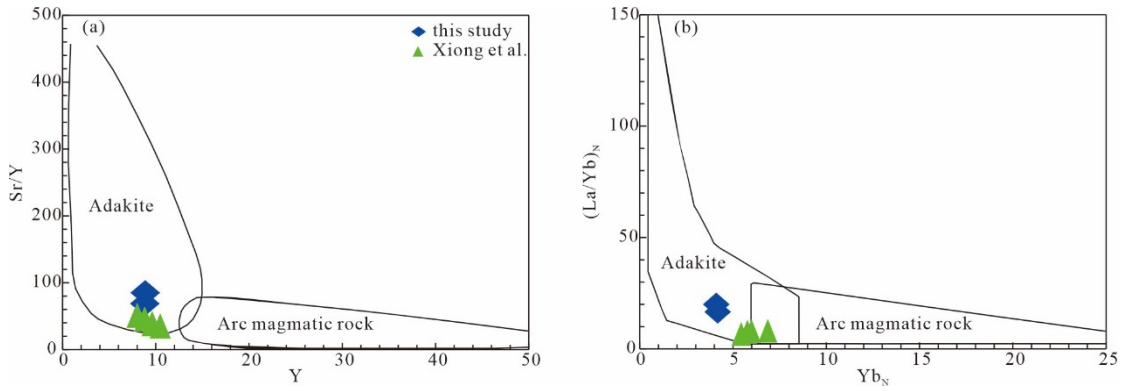

Figure 7. Diagrams of (**a**) Sr/Y–Y and (**b**) (La/Yb)N–(Yb)N for granitoids in Baiyinhushuo (after [37]).

The $Mg^{\#}$ of adakite is an important parameter for determining the origin of magma, and experimental petrological studies have confirmed that the $Mg^{\#}$ formed by partial melting of dehydrated basaltic rocks is usually lower than 45 [38]. High-Mg adakitic rocks are generally believed to be formed by partial melting of the thickened lower crust of after detachment and interaction with mantle peridotite [39], or by melting of subducted oceanic crust and interacted with mantle wedge [40], and some scholars also believe that they are formed by the mixing of mantle-derived basic magma and crustal acidic magma [41].

 doi:10.20944/preprints202406.0702.v1

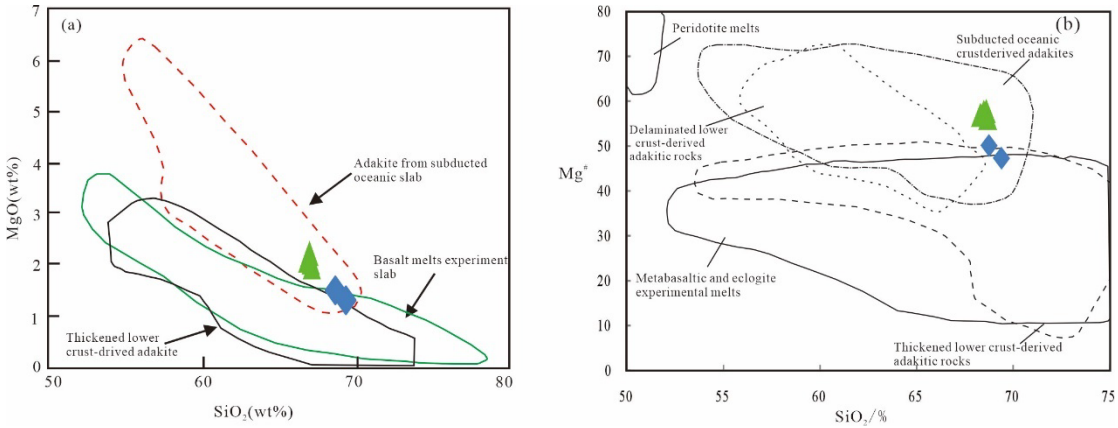

Figure 8. SiO2-Mg# (**a**) diagram and SiO2-MgO diagram (**b**) for the in Baiyinhushuo area (after [42]).

The Mg# of the Baiyinhushuo adakite ranges from 46.73 to 61.78, with an average value of 56.14, which is higher than that of the adakite formed by partial melting of the MORB, and also higher than that of the adakite derived from lower crustal melting, such as the Mg# of the adakites range from about 35.72 to 46.16 formed by underplating in the North China Craton [43–45]. In the MgO- SiO_2 diagram (Figure 8), the samples fall in the field of subducted slab-derived adakitic rocks, indicating that the source of Baiyinhushuo adakite is subducted slab of CAOB. In addition, the adakites derived thickened lower crust- are often Na-rich and K-poor, and belong to the peraluminous magma [42], while the adakite of Baiyinhushuo have the characteristics of K-rich and Na-poor, which is different from the adakites derived from the lower crust.

The high-Mg adakitic andesite of Early Triassic (244 Ma) was also discovered in the adjacent Linxi region, which derived from the partial melting of the remnant oceanic slab preserved in the mantle of the subduction zone [46], and is similar to the geochemical characteristics of the Baiyinhushuo adakite. Therefore, we believe that the Baiyinhushuo adakite was most likely generated by partial melting of subducted oceanic crust.

The adakitic rocks were enriched in large ion lithophile elements (LILEs, such as Th and Rb) and depleted in Nb, Ta, Ti, and P, reflecting the geochemical characteristics of the subduction zone. In the (Yb+Ta)-Rb diagram and (Y+Nb)-Rb diagram, all samples also fall into the field of volcanic arc granite, indicating that the adakite are most likely emplaced at island arc background (Figure 9).

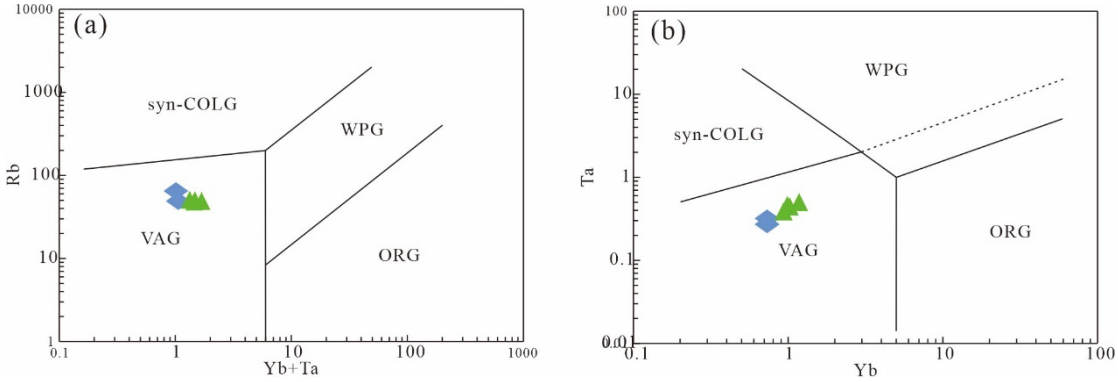

Figure 9. (**a**) Rb-(Y+Nb) and Rb-(Yb+Ta) tectonic discriminant diagrams of the Baiyinhushuo (modified from [47]).

The igneous rocks derived from the melting of the lower crust exhibits distinct crustal characteristics in terms of isotopes, while the magma rock derived from the melting of subducted oceanic crust inevitably carries the signature of the oceanic crust. It is generally believed that the magma with Sr-Nd isotopic characteristics close to MORB directly derived from the melting of oceanic crust.

 doi:10.20944/preprints202406.0702.v1

Generally, Sr-Nd isotopic signatures of magmas close to MORB are directly derived from the melting of mantle-derived oceanic crust (MORB), which is related to the island arc setting of the subduction zone. If $(^{87}Sr/^{86}Sr)i > 0.704$, typically between 0.706 and 0.710, it is considered that the magma derived from the partial melting of the basalt of juvenile lower crust caused by underplating, which is closely related to the intracontinental post-collision tectonic environment during the thickening lithosphere delamination and mantle magma underplating [48–50]. The Baiyinhushuo adakite has a low $(^{87}Sr/^{86}Sr)i$ (0.703382), high $^{143}Nd/^{144}Nd$ (0.512721) and $\varepsilon_{Nd(t)}$ values (+7.72). In the Sr-Nd isotope diagram (Figure 10), the samples fall in the field of subducted oceanic adakite, far from the fields that thicked lower crust-derived. The Sr-Nd isotopes show that the source region is close to the depleted mantle, with a two-stage model age of 387 Ma, It exhibits a close affinity to the Sr-Nd isotopic values of the ophiolite in the adjacent Xi Ujimqin region, suggesting isotopic characteristics are similar to those of subducted oceanic crust. Therefore, the Baiyinhushuo adakite derived from the partial melting of subducted oceanic crust, with its source potentially being the break-off subducted oceanic crust of CAOB.

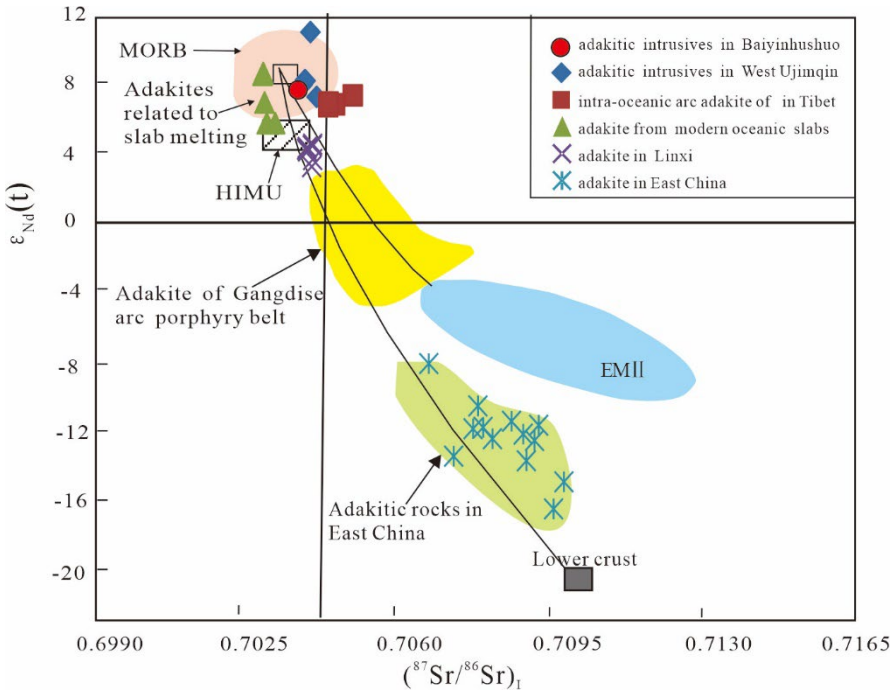

Figure 10. $(^{87}Sr/^{86}Sr)_i$ –$\varepsilon_{Nd}(t)$ isotope composition of Baiyinhushuo (after [51]). Date sources: intra-oceanic adakite of Tibet is from [49]; adakite of modern intra-oceanic arc is from [52,53]; adakite in Linxi is from [8].

The high stability of zircon, along with its high Hf mass fraction and very low $^{176}Lu/^{177}Hf$, and the fact that it crystallizes with little or no radiogenic Hf accumulation, make zircon Hf isotope studies one of the most important means of tracing magma source at present [34,54]. The $\varepsilon_{Hf(t)}$ in the Baiyinhushuo adakite are all positive, with a small range of variation between 11.3 and 13.8, and all points are located between the evolutionary line of depleted mantle and the chondrite (Figure 10), and the Hf isotopic signature is consistent with the evolution of Hf in mantle-derived magma in the eastern region of the Xing-Meng orogenic belt (Figure 11) [8,55], showing similar isotopic composition characteristics to Phanerozoic magmatic rocks in the eastern part of Xing-Meng orogenic belt. The two-stage model age of zircon Hf isotopes is 323-459 Ma, which is relatively young, implying that the Early Paleozoic subducted oceanic crust. is important in the magma genesis.

 doi:10.20944/preprints202406.0702.v1

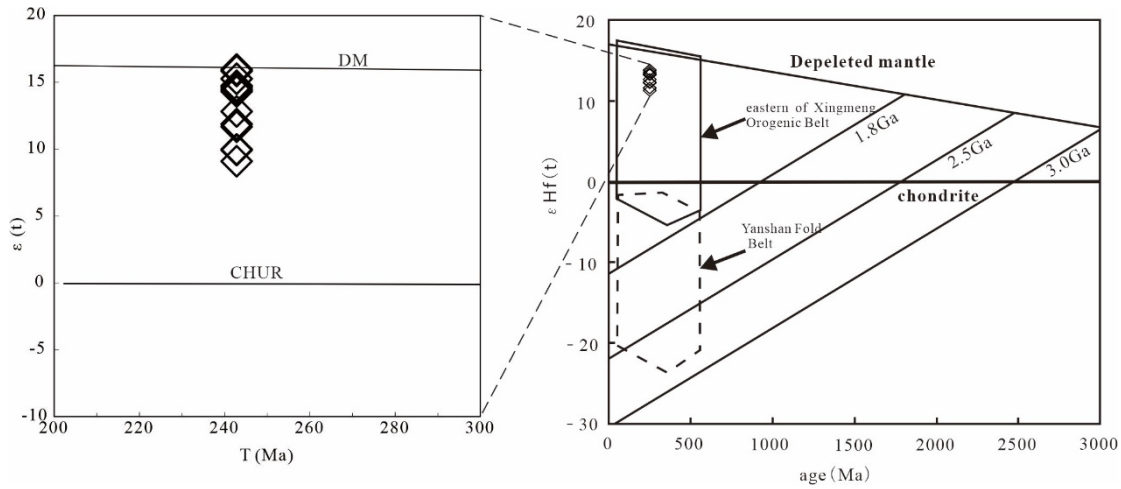

Figure 11. ε_{Hf} (t)-T diagram of zircon (after [55]).

5.3. Tectonic Implications

The Late Permian-Early Triassic was a key stage in the tectonic evolution of the Central Asian Orogenic Belt (CAOB), in which the paleo-Asian Ocean closed and changed from subduction accretion to collisional orogeny. Previous research on the sedimentology and paleogeography of the Late Permian Linxi Formation in the southern segment of the Daxing'anling Mountains show that the region was marine sediment in the early-middle stage of the Late Permian as a remnant basin, and it was not until the late stage transitioned to a terrestrial environment. In the early Triassic, river lake facies sedimentary layers with red layer properties appeared [56], indicating that the surface of the paleo-Asian Ocean had closed.

In the Early Triassic, although the surface of the Paleo-Asian Ocean was closed, a large number of adakites derived from the melting of subducted slab in the area north of the Xar Moron suture zone. For example, the Early Mesozoic (244 Ma) high-Mg adakitic andesite exposed in the Linxi region derived from the partial melting of the residual oceanic crust preserved in the mantle beneath the paleo-subduction zone, followed by interaction with mantle peridotite [46]. Li et al. (2020) [17] concluded that the volcanic rock of Lower Triassic Xingfuzhilu Formation (247 Ma) in the Linxi area is a typical adakite derived from the melting of oceanic slabs, and that subducted oceanic slabs still existed during the Early-Middle Triassic after the closure of the paleo-Asian Ocean surface. According to detailed zircon mineral study, Liu et al. (2007) [57] concluded that the adakitic rocks of the Longtoushan pluton (241 Ma) hydrous mafic rocks of the subducted oceanic crust. Shao et al. (2002) [58] analyzed the Sr-Nd isotopic characteristics of various igneous rocks and combined them with geophysical data, suggesting that the Mesozoic "soft collision, weak orogenesis" tectonic environment allowed a considerable portion of the oceanic plates to remain in the crust-mantle transition zone rather than completely returning to the asthenosphere, indicating that lithospheric-scale subduction continued.

Additionally, in the region of Xilinhot-Xi Ujimqin region, the Early Triassic dacite-rhyolite has been discovered in the volcanic rock sections of the Dalinuoer Formation and the Baoeraobao Formation. These rocks age of petrogenesis were 245.7±1.8Ma and 242.7±4.0Ma (K-Ar whole-rock ages, [59]), exhibiting geochemical characteristics similar to A-type granites. They belong to the extrusive phase of the contemporaneous A-type calc-alkaline series of peraluminous-type granites, closely related to the continental crust extension process resulting from the underplating of mantle-derived magma.

During the Late Permian to Early Triassic, the subduction plate segment of the Paleo-Asian Ocean broke-off, and the remnant oceanic crust preserved in the mantle of the Paleo-subduction zone still underwent partial melting, generating adakitic magma. Concurrently, the asthenospheric mantle upwelling, causing the melting of materials at different depths within the lithosphere, resulting in

 doi:10.20944/preprints202406.0702.v1

the petrogenesis of both adakitic rocks with island arc characteristics and rock assemblages under an extensional setting in the subduction zone

5. Conclusions

(1) The emplacement age of the Baiyinhushuo adakite granodiorite in the southeast of the Central Asian Orogenic Belt is 242.8±Ma, corresponding to the Early Triassic, and its geochemistry exhibits the characteristics of adakite.

(2) The Baiyinhushuo adakite has low $(^{87}Sr/^{86}Sr)_i$ and high $\varepsilon_{Nd(t)}$ values, and they may derived from partial melting of the broken-off subducted oceanic crust, which interacted with the mantle in the process of uplift beneath the subduction zone.

(3) The Late Permian-Early Triassic period marks a crucial stage in the tectonic transition from subduction to collisional orogeny. In this region, due to the slab break-off and the asthenosphere upwelling, the materials at different depths melt, forming the rock assemblages in diverse tectonic environments.

Author Contributions: Conceptualization and methodology, Y.F. and Q.X.; formal analysis, Y.F. and Q.X.; investigation, Y.F., Y.C. and Y.L.; resources, Y.C. and Q.X.; data curation, Y.F.; writing-original draft preparation, Y.F.; writing-review and editing, Y.F. and Q.X.; funding acquisition, Q.X. All authors have read and agreed to the published version of the manuscript.

Funding: This work was financially supported by the Geological Prospecting Foundation of Inner Mongolia Autonomous Region of China (Project No. 2017-YS01) and (Project No. 2020-YS01).

Data Availability Statement: The data set is presented directly in the present study.

Acknowledgments: We sincerely appreciate the State Key Laboratory Laboratory of Mineral Deposits Research, Nanjing University and the Key Laboratory of Continental Dynamics of Ministry of Natural Resources for helping with experimental analysis.

Conflicts of Interest: The authors declare no conflict of interest.

References

1. Sengör.A.M.C.. Natalin.B.A.. Burtman. V.S..1993. Evolu-tion of the Altaid Tectonic Collage and Paleozoic Crus-tal Growth in Eurasia. Nature ,364 :299 -307.
2. Sengör A M C, Natal'In B A. Turkic-type orogeny and its role in the making of the continental crust. Annual Review of Earth and Planetary Sciences, 1996, 24(1): 263-337.
3. Xiao, W.J., Brian F. Windley, Hao, J., Zhai. M.G., 2003. Accretion leading to collision and the Permian Solonker suture, Inner Mongolia, China: Termination of the central Asian orogenic belt. Tectonics 22(6):n/a-n/a.
4. Xiao, W.J., Windley, B.F., Han, C.M., Liu, W., Wan, B., Zhang, J.E., Ao, S.J., Zhang, Z.Y., Song, D.F. 2018. Late Paleozoic to Early Triassic multiple roll-back and oroclinal bending of the Mongolia collage in Central Asia. Earth-Science Reviews, 186: 94-128.
5. Xiao, W.J, Song, D.F., Windley, B.F., Li, J.L., Han, C.M., Wan, B., Zhang, J.E., Ao, S.J. Zhang, Z.Y. 2020. Accretionary processes and metallogenesis of the Central Asian Orogenic Belt: Advances and perspectives. Science China (Earth Sciences), 63(3): 329-361.
6. Windley B F, Alexeiev D, Xiao W J, Kröner A, Badarch G. 2007.Tectonic models for accretion of the central Asian orogenic belt. J Geol Soc, 164: 31–47.
7. Liu J.F., Chi X.G., Zhan Z., Hu Z.C. and Chen J.Q. 2013. Zircon U-Pb age and petrologenetic discussion on Jianshetun adakite in Balinyouqi, Inner Mongolia. Aeta Petrologica Sinica,29(3): 827 -839 (in Chinese with English abstract).
8. Liu J.F., Li J.Y., Chi X.C., Qu J.F., Hu Z.C. and Guo C.L. 2014. Petrological and geochemical characteristics of the Karly 'Triassic granite belt in southeastern Inner Mongolia and its tectonic setting. Acta Ceologioa Sinica,88(9): 1677 -1690 (in Chinese with English abstract).
9. Liu, J.F., Li, J.Y., Chi, X.G., Qu, J.F., Chen, J.Q., Hu, Z., and Feng, Q.W. 2016. The tectonic setting of early Permian bimodal volcanism in central Inner Mongolia: Continental rift, post-collisional extension, or active continental margin? International Geology Review, 58(6): 737–755.
10. Liu J.F., Li J.Y., Zhao S., Zhang J., Zheng R.G., Zhang W.L., Lv Q.L., Zheng P.X. 2022. Crustal accretion and Paleo-Asian Ocean evolution during Late Paleozoic-Early Mesozoic in southeastern Central Asian Orogenic Belt: Evidence from magmatism in Linxi-Dongwuqi area, southeastern Inner Mongolia. Acta Petrologica Sinica, 38(8): 2181-2215. https://doi.org/10.18654/1000-0569/2022.08.02.

 doi:10.20944/preprints202406.0702.v1

11. Li, Y.J., Wang, J.F., Li, H.Y.; et al., 2012. Recognition of Diyanmiao Ophiolite in Xi Ujimqin Banner, Inner Mongolia. Acta Petrologica Sinica, 28(4):1282-1290(in Chinese with English abstract).
12. Li, Y.J., Wang, J.F., Wang, G.H., Li, H.Y., Dong, P.P., 2018. Discovery and significance of the Dahate fore-arc basalts from Diyanmiao ophiolite in Inner Mongolia. Acta Petrobgica Sinica, 34 (02):469-482.
13. Cheng, Y., Xiao, Q.H., Li, T.D.; et al., 2019. Magmatism and Tectonic Background of the Early Permian Intra-Oceanic Arc in the Diyanmiao Subduction Accretion Complex Belt on the Eastern Margin of the Central Asian Orogenic Belt. Science China:Earth Sciences, 44(10):3454-3468(in Chinese with English abstract).
14. Li S., Chung S. L., Wilde S. A., Jahn B. M., Xiao W. J., Wang T, Guo Q. Q. 2017. Early-Middle Triassic high Sr/Y granitoids in the southern Central Asian Orogenic Belt: Implications for ocean closure in accretionary orogens. Geophys Res Solid Earth, 122: 2291–2309.
15. Xiong, G.Q., Liu, M., Zhao, H.T., Zhang, D., Wang, H.R., Wang, Z., Hu, X.C. 2015. Zircon U-Pb .LA-ICP-MS dating, geochemical, Hf isolopic characteristics of Bayanhushu granodiorite in West Ujimqin banner and geological significance. Geological Review.G1(3): 651 -663. (in Chinese with English abstract).
16. Fan, Y.X., Li, T.D., Xiao, Q.H., Cheng, Y., Li Y., Guo, L.J., Luo, P.Y. 2019. Zircon U-Pb ages，geochemical characteristics of Late Permian granite in West Ujimqin Banner, Inner Mongolia, and tectonic significance. Geological Review, 65(1); 248 -266 (in Chinese with English abstract).
17. Li, S.C.，Wang, H.T.，Li, G.，Wang, X.A.，Yang, X.P., Zhao, Z.R. 2020. Northward plate subduction process of the Paleo-Asian Ocean in the middle part of the Central Asian Orogenic Belt: Evidence from adakites. Acta Petrologica Sinica，36(8) : 2521-2536. https://doi.org/10. 18654 /1000-0569 /2020. 08. 14.
18. Li, S., Chung, S. L., Wilde, S.A., Wang, T., Xiao, W.J., Guo, Q.Q. 2016. Linking magmatism with collision in an accretionary orogen. Sci Rep, 6: 25751.
19. Wu, D.D., Li, S., Chew, D., Liu, T.Y., Guo, D.H. 2021. Permian-Triassic magmatic evolution of granitoids from the southeastern Central Asian Orogenic Belt: Implications for accretion leading to collision. Science China Earth Sciences, 64(5): 788–806. https://doi.org/10.1007/s11430-020-9714-5.
20. Miao, L.C., Zhang, F., Fan, W.M., and Liu, D.Y. 2007. Phanerozoic evolution of the Inner Mongolia–Daxinganling orogenic belt in North China: Constraints from geochronology of ophiolites and associated formations. Geological Society, London, Special Publications, 280(1): 223–237. https://doi.org/10.1144/SP280.11.
21. Wang, J.F., Li, Y.J., Li, H.J., and Dong, P.P. 2017. Discovery of Early Permian Intra-oceanic arc adakite in the Meilaotewula Ophiolite, Inner Mongolia and its evolution model. Acta Geologica Sinica, 91(8): 1776–1795.
22. Liu Y.S., Hu Z.C., Gao S., Günther D., Xu J., Gao C.G. and Chen H.H., 2008. In situ analysis of major and trace elements of anhydrous minerals by LA-ICP-MS without applying an internal standard. Chem. Geol., 257(1-2): 34-43. https://doi.org/10.1016/j.chemgeo.2008.08.004.
23. Ludwig.K.R. 2003. Users Manual for Isoplot 3.00; A Geo-chronological Toolkit for Microsoft Excel. Berkeley Ge-ochronolog y Center, Special Publication,4:1-71.
24. Hou K.J.，Li Y.H.，Zou T.R.，Qu X.M.，Shi Y.R.，Xie G.Q. 2007. Laser ablation-MC-ICP-MS technique for Hf isotope microanalysis of zircon and its geological applications. Acta Petrologica Sinica, 23(10): 2595-2604.
25. Scherer, E., Munker, C., Mezger, K., 2001. Calibration of the lutetium-hafnium clock. Science, 293 (5530):683-687.
26. Blichert-Toft, J., Albarède, F., 1997. The Lu-Hf Isotope Geochemistry of Chondrites and the Evolution of the Mantle-Crust System. Earth and Planetary Science Letters, 148(1/2):243-258. https://doi.org/10.1016/s0012-821x(97)00040-x.
27. Corfu, F., Hanchar, J.M., Hoskin, P.W.O.; et al., 2003. Atlas of Zircon Textures. Reviews in Mineralogy and Geochemistry, 53(1):469-500. https://doi.org/10.2113/0530469.
28. Wu, Y. B., Zheng, Y. F., 2004. Genesis of Zircon and its Constraints on Interpretation of U-Pb Age. Chinese Science Bulletin, 49(15):1554-1569(in Chinese with English abstract). https://doi.org/10.1007/BF03184122.
29. Middlemost, Eric.A.K., 1994. Naming materials in the magma/igneous rock system. Earth-Science Reviews, 37 (3):215-224.
30. Maniar, P.D., Piccoli, P.M., 1989. Tectonic discrimination of granitoids. GSA Bull, 101: 635-643.
31. Peccerillo, A.; Taylor, S.R. Geochemistry of eocene calc-alkaline volcanic rocks from the Kastamonu area, Northern Turkey. Contrib. Fan Miner. Petrol. 1976, 58, 63–81.
32. Miyashiro, A.. 1974． Volcanic rock series in island arcs and active continental margins． American Journal of Science，274: 321～ 355.
33. Sun, S.S., McDonough, W.E.. 1989. Chemical and Isotopic Systematics of Oceanic Basalts: Implications for Mantle Composition and Processes. In: Saunders, A.D., Norry, M.J., eds., Magmatism in the Ocean Basins, Geological Society of London, Specialcation, London, 313-345.
34. Wu, F.Y., Li, X.H., Zheng, Y.F.; et al., 2007. Lu-Hf Isotopic Systematics and their Applications in Petrology. Acta Petrologica Sinica, 23(2):185-220(in Chinese with English abstract) ttp://www.wanfangdata.com.cn/details/detail.do?_type=perio&id=ysxb98200702001.

35. Bao, Q.Z., Zhang, C.J., Wu, Z.L., Wang H., Li W., Sang J.H.. 2007. SHRIMP U-Pb Zircon Geochronology of a Carboniferous Quartz-Diorite in Baiyingaole Area, Inner Mongolia and Its Implications. Journal of Jilin University (Earth Science Edition), 37(1):15-23(in Chinese with English abstract).
36. Guo, Z.J., Zhou Z.H., Li G.T., Li J.W., Wu X.L., Ouyang H.G., Wang A.S., Xiang A.P., Dong X.Z.. 2012. SHRIMP U-Pb zircon dating and petrogeochemistral characteristics of the intermediate-acid intrusive rocks in the Aoergai copper deposit of Inner Mongolia. Geology in China,39(6):1486 -1500 (in Chinese with English abstract).
37. Defant M J., Drummond M S.1990. Derivation of some modern arc magmas by melting of young subducted lithosphere. Nature 347:662.
38. Rapp, R. P., N. Shimizu, M. D. Norman, G. S. Applegate.1999. Reaction between slab-derived melts and peridotite in the mantle wedge: Experimental constraints at 3.8 GPa. Chemical Geology 160(4):335-356.
39. Martin, H., Smithies, R.H., Rapp, R., Moyen, J.F. 2005. An overview of adakite, tonalite-trondhjemite-granodiorite (TTG),and sanukitoid: Relationships and some implications for crustal evolution. Lithos, 79(1/2):1-24.
40. Kelemen, P.B., 1995. Genesis of High $Mg^{\#}$ Andesites and the Continental Crust. Contributions to Mineralogy and Petrology, 120(1): 1-19.
41. Chen, B., Jahn, B.M., Wilde, S.A., and Xu, B. 2000. Two contrasting Paleozoic magmatic belts in northern Inner Mongolia, China: Petrogenesis and tectonic implications. Tectonophysics, 328(1–2): 157–182.
42. Wang, Q., Xu, J.F., Jian, P., Bao, Z.W., Zhao, Z.H., Li, C.F.; et al. 2006. Petrogenesis of adakitic porphyries in an extensional tectonic setting, Dexing, South China: Implications for the genesis of porphyry copper mineralization. Journal of Petrology, 47: 119–144.
43. Zhang Q., Wang Y., Qian Q., Yang J.H., Wang Y.L., Zhao T.P., Guo G.J. 2001. The characteristics and tectonic-metallogenic significances of the adakites in Yanshanian period from eastern China. Acta Petrologica Sinica, 17(2): 236- 244.
44. Luo H.L., Wu T.R., Li Y. 2007&. Geochemistry and SHRIMP dating of the Kebu massif from Wulatezhongqi, Inner Mongolia: Evidence for the Early Permian underplating beneath the North China Craton. Acta Petrologica Sinica, 23(4):755~766.
45. Xiong X.L., Liu X.C., Zhu Z.M., Li Y., Xiao W.S., Song M.S., Zhang S., Wu J.H. 2011. Adakitic rocks and destruction of the North China Craton: Evidence from experimental petrology and geochemistry. Science China (Earth Science), 54: 858-870.
46. Wang, D. B., Liu, Y. S., Zong, K. Q.; et al., 2009. Early Mesozoic O-Type High-Mg Adakitic Andesites from Linxi Area, Inner Mongolia and Its Implication. Geological Science and Technology Information, 28(6): 31-38(in Chinese with English abstract). http://www.en.cnki.com.cn/Article_en/CJFDTOTAL-DZKQ200906005.htm.
47. Pearce J A, Harris N B W, Tindle A G.1984.Trace element discrimination diagrams for the tectonic interpretation of granitic rocks. Journal of Petrology, 25(4):956~983.
48. Zhao, Z.H., Wang, Q., Xiong, X.L.; et al., 2006. Two-Types of Adakites in North Xinjiang China. Acta Petrologica Sinica, 22(5):1249-1265(in Chinese with English abstract).
49. Hou, Z.Q., Pan, X.F., Yang, Z.M.; et al., 2007.Porphyry Cu Mo-Au)Deposits no Related to Oceanic-Slab Subduction:Examples from Chinese Porphyry Deposits in Continental Settings.Geoscience, 21(2):332-351(in Chinese with English abstract).
50. Wei, D. L., Xia, B., Zhou, G. Q.; et al., 2007. Geochemistry and Sr-Nd Isotope Characteristics of Tonalites in Zêtang, Tibet:New Evidence for Intra-Tethyan Subduction. Science in China Series D: Earth Sciences, 50(6):836-846(in Chinese). https://doi.org/10.1007/s11430-007-0034-8.
51. Hou, Z. Q., Gao, Y. F., Qu, X. M.; et al., 2004. Origin of Adakitic Intrusives Generated during Mid-Miocene East-West Extension in Southern Tibet. Earth and Planetary Science Letters, 220(1/2):139-155. https://doi.org/10.1016/s0012-821x(4)00007-x.
52. Falloon, T.J., Danyushevsky, L.V., Crawford, A.J., Meffre, S., Woodhead, J.D.,Bloomer, S.H., and 49(4): 697–715. https://doi.org/10.1093/petrology/egm080.
53. Li, Y.B., Kimura, J.I., Machida, S., Ishii, T., Ishiwatari, A., Maruyama, S.; et al.2013. High-Mg adakite and low-Ca boninite from a bonin fore-arc seamount: Implications for the reaction between slab melts and depleted mantle. Journal of Petrology, 54(6): 1149–1175. https://doi.org/10.1093/petrology/egt008.
54. Amelin, Y., Lee, D. C., Halliday, A. N.; et al., 1999. Nature of the Earth's Earliest Crust from Hafnium Isotopes in Single Detrital Zircons. Nature, 399(6733):252-255. https://doi.org/10.1038/20426.
55. Yang J.H., Wu F.Y., Shao J., Wilde S. A., Xie L.W., Liu X.M. 2006. Constraints on the timing of uplift of the Yanshan Fold and Thrust Belt, North China. Earth and Planetary Science Letters 246(3):336~352.
56. He Z.J., Liu S.W., Ren J.S., Wang Y. 1997. Later Permian-early Trissic sedimentary evolution and tectonic setting of Linxi region Inner Mongolia.Regional Geology of China,16(4):403~409.
57. Liu W., Pan X.F., Xie L.W., Li H. 2007. Sources of material for the Linxi granitoids, the southern segment of the Da Hinggan Mts.: When and how continental crust grew?.Acta Petrologica Sinica, 23(2):441-460.

 doi:10.20944/preprints202406.0702.v1

58. Shao J.A., Hong D.W., Zhang L.Q. 2002: Genesis of Sr-Nd isotopic characteristics of igneous rocks in Inner Mongolia. Geological Bulletin of China, 21(12): 817-822.
59. Zhang X.H., Zhang H.F., Tang Y.J., Liu J.M. 2006. Early Triassic A-type felsic volcanism in the Xilinhaote-Xiwuqi, central Inner Mongolia: Age, geochemistry and tectonic implications. Acta Petrologica Sinica, 22(11): 2769-2780.